A new mitofusin topology places the redox-regulated C terminus in the mitochondrial intermembrane space

Sevan Mattie,[1] Jan Riemer,[2] Jeremy G. Wideman,[3,4] and Heidi M. McBride[1]

[1]Montreal Neurological Institute, McGill University, Montreal, Quebec, Canada
[2]Institut für Biochemie, University of Cologne, Köln, Germany
[3]Biosciences, University of Exeter, Exeter, England, UK
[4]Wissenschaftskolleg zu Berlin, Berlin, Germany

Mitochondrial fusion occurs in many eukaryotes, including animals, plants, and fungi. It is essential for cellular homeostasis, and yet the underlying mechanisms remain elusive. Comparative analyses and phylogenetic reconstructions revealed that fungal Fzo1 and animal Mitofusin proteins are highly diverged from one another and lack strong sequence similarity. Bioinformatic analysis showed that fungal Fzo1 proteins exhibit two predicted transmembrane domains, whereas metazoan Mitofusins contain only a single transmembrane domain. This prediction contradicts the current models, suggesting that both animal and fungal proteins share one topology. This newly predicted topology of Mfn1 and Mfn2 was demonstrated biochemically, confirming that the C-terminal, redox-sensitive cysteine residues reside within the intermembrane space (IMS). Functional experiments established that redox-mediated disulfide modifications within the IMS domain are key modulators of reversible Mfn oligomerization that drives fusion. Together, these results lead to a revised understanding of Mfns as single-spanning outer membrane proteins with an N_{out}–C_{in} orientation, providing functional insight into the IMS contribution to redox-regulated fusion events.

Introduction

In animals, mitochondrial fusion is activated during cellular stress and starvation, events that render the cells refractive to apoptosis and protect the mitochondrial reticulum from autophagy (Shutt and McBride, 2013). However, the precise molecular mechanisms that drive mitochondrial fusion have not been established. Although mitochondrial fusion has been observed in diverse eukaryotes, the machinery driving fusion has been identified only in opisthokonts, the lineage comprising animals and fungi. Two dynamin domain–containing proteins are required for mitochondrial fusion in mammals: Mfn1/Mfn2 in the outer mitochondrial membrane and Opa1 in the inner mitochondrial membrane (Labbé et al., 2014). Although the orthology of fungal Fzo1 to Mfns and fungal Mgm1 to Opa1 has been assumed based on domain organization and similarity of function, sequence-based orthology detection methods fail to retrieve these orthologue sets (Muñoz-Gómez et al., 2015; Purkanti and Thattai, 2015). Loss of any of these genes leads to mitochondrial fragmentation, and mouse models lacking Mfn1, Mfn2, or Opa1 are embryonic lethal (Chen et al., 2003; Davies et al., 2007; Pareyson et al., 2015). Cell-free fusion assays developed in both *Saccharomyces cerevisiae* and mammalian systems have identified core principles of mitochondrial fusion, namely that the process depends on GTP hydrolysis, that these GTPases are each essential for fusion, and that cytosolic factors can promote fusion (Meeusen et al., 2004, 2006; Schauss et al., 2010; Hoppins et al., 2011; Shutt et al., 2012; Mishra et al., 2014). In the mammalian system, mitochondrial fusion is activated upon cellular stress, where oxidized glutathione disulfide (GSSG) promotes the assembly of higher-order Mfn complexes mediated by reversible disulfide bonds (Shutt et al., 2012). The cysteine residues responsible for these dynamic oligomers were located within the C-terminal domain, assumed to be a cytosol-exposed region. Oligomerization occurred in cis, before mitochondrial docking, suggesting that the generation of disulfide-induced Mfn2 oligomers may act to "prime" them to bind in trans and drive mitochondrial fusion (Ryan and Stojanovski, 2012; Shutt et al., 2012). A confounding element of this previous work is that the cytosol is generally considered a reducing environment, making it difficult to envision how GSSG-induced redox switching may occur within a cytosolic domain. In this study, we revisit the topology of Mfn1 and Mfn2 by validating bioinformatic predictions with biochemical and functional experiments. The data lead to a revised model of holozoan mitofusins as N_{out}–C_{in} proteins, consisting of a single membrane-spanning domain (transmembrane domain [TMD]) with the 110 residue containing heptad repeat 2 (HR2) and metazoan-specific disulfide-modifiable cysteine residues residing within the intermembrane space (IMS).

Correspondence to Heidi M. McBride: heidi.mcbride@mcgill.ca; Jeremy G. Wideman: jeremy.grant.wideman@gmail.com

The Rockefeller University Press
J. Cell Biol. Vol. 217 No. 2 507–515
https://doi.org/10.1083/jcb.201611194

Results and discussion

Holozoan Mfns and fungal Fzo1 are divergent dynamin domain–containing proteins with distinct domain architecture

To better map the conserved functional domains within Mfns and Fzo1, we collected homologous protein sequences from diverse animal and fungal genomes (Table S1). Surprisingly, initial searches using Basic Local Alignment Search Tool (BLAST) suggested that certain bacterial dynamin-like proteins (BDLPs) might be more closely related to Mfn or Fzo than Mfn and Fzo are to each other or to other eukaryotic dynamin-like proteins. Phylogenetic reconstruction of the GTPase domains from Fzos, Mfns, and BDLPs provided no strong support for the relationship of Mfn or Fzo to particular bacterial sequences or to one another (Fig. 1 A and Fig. S1, A and B). These data suggest either that (a) Mfns are as related to Fzos as either are to BDLPs (e.g., Mfn and Fzo arose from separate horizontal gene transfers), or (b) more likely, in the time since the divergence of animals and fungi, the sequences of Mfn and Fzo have diverged from a common ancestral protein so much that the evolutionary history of these proteins cannot be adequately assessed by current phylogenetic methods.

Examining predicted functional domains revealed that Mfn and fungal Fzo have similar predicted N-terminal dynamin GTPase domains and at least two predicted coiled-coil regions, so-called HR1, located near the middle of the protein, and HR2 at the very C terminus (Fig. 1 B). However, the C-terminal regions of Mfns and Fzos have no detectable sequence similarity and cannot be reliably aligned. Bioinformatic predictions showed that Mfn proteins carry only a single predicted C-terminal TMD, whereas fungal Fzo1 proteins have two predicted C-terminal TMDs (Fig. 1 B).

Because the C-terminal domain of Mfns is redox regulated, we performed a manual inspection of conserved cysteine residues within this region. There was a striking correlation between the emergence of multicellular animals (metazoans) with the appearance of a single TMD and the conserved cysteines (Fig. 1 C, yellow residues). All metazoans analyzed contain one or more Mfn paralogues that contain at least one of the two conserved cysteine residues, whereas the unicellular holozoan relatives of animals (e.g., choanoflagellates and filasterians) lack cysteines at the conserved sites (Fig. 1 C). This result suggests that stress-induced mitochondrial fusion may be a specific adaptation to multicellular life. However, some unicellular holozoans do contain cysteines at nonhomologous sites in the C-terminal region, indicating some degree of sequence convergence (Fig. 1 C, red residues). Manual inspection of the C-terminal region of fungi did not reveal any conserved cysteine residues.

Homo sapiens Mfn1 and Mfn2 C terminus is exposed to the mitochondrial IMS

To directly interrogate the topology of endogenous Mfn2, we performed protease protection experiments on mitochondria isolated from HEK293 cells, using specific antibodies to detect endogenous Mfn2. We mapped and confirmed the precise epitopes of two available antibodies (Cell Signaling Technology and Abnova) using recombinant proteins (Fig. S2, A and B). The Cell Signaling Technology antibody recognized an epitope immediately upstream of the conserved TMD corresponding to residues V_{573} to S_{585}, and the Abnova antibody was specific to residues C-terminal to the TMD domain, residues

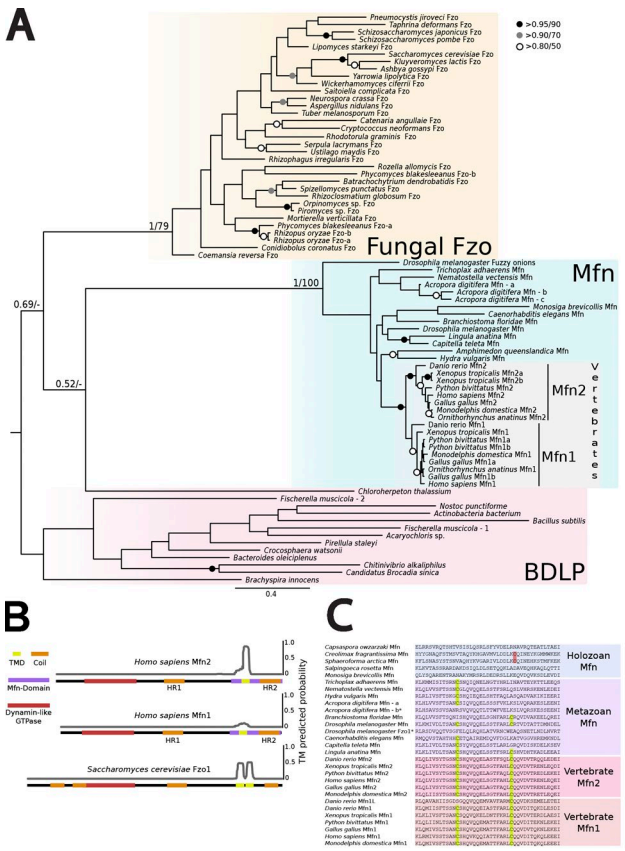

Figure 1. **Bioinformatic analysis of Fzo and Mfn. (A)** Phylogenetic reconstruction of dynamin domain–containing proteins from bacteria, fungi, and animals. Fzo1- and Mfn-like sequences collected by BLAST (Altschul et al., 1997) and HMMer (Eddy, 2011) searches were aligned and subjected to phylogenetic reconstruction using MrBayes v3.2 (Ronquist and Huelsenbeck, 2003) and RaxML v8.2 (Stamatakis, 2006; Fig. S1 A). Long-branching bacterial sequences were removed from the dataset to decrease the effects of long-branch attraction (Fig. S1 B). Degenerate paralogues of Fzo1 in fungi lacking normal mitochondria were removed to generate the phylogenetic reconstruction depicted. Support values are as inset. The topology shown is from the MrBayes analysis. **(B)** Domain organization of *S. cerevisiae* Fzo1 and *H. sapiens* Mfn1 and Mfn2. TMDs and coiled-coil domains were predicted using TMHMM2.0 (Krogh et al., 2001) and COILS (Lupas, 1996), respectively. **(C)** Alignment of Mfn proteins highlighting conserved cysteine residues putatively involved in oligomerization. Mfn proteins were aligned using MUSCLE (Edgar, 2004) and manually inspected to identify conserved cysteine residues.

661–757 (Fig. 2 A and Fig. S2 A). Increasing amounts of trypsin from 10 to 500 µg/ml revealed a highly protected, ∼20-kD C-terminal fragment of Mfn2 that was seen with both antibodies, which was degraded upon addition of detergent (Fig. 2 B and Fig. S2, B, C, and F). Because the Cell Signaling Technology epitope is predicted to reside on the cytosolic face of the mitochondrial outer membrane, we next used proteinase K to completely degrade all exposed amino acids, which then led to a loss of this epitope and appearance of a shorter, ∼15-kD protected fragment recognized only by the Abnova antibody (Fig. 2 C). This epitope was proteinase K accessible after treatment with either detergent or hypotonic shock (Fig. 2 C). In further agreement with the bioinformatic analysis, an antibody specific to the very C terminus of Mfn1 (residues 665–741; Santel et al., 2003) also revealed a ∼15-kD proteinase K protected fragment, accessible only in the presence of detergent or hypotonic shock (Fig. 2 D).

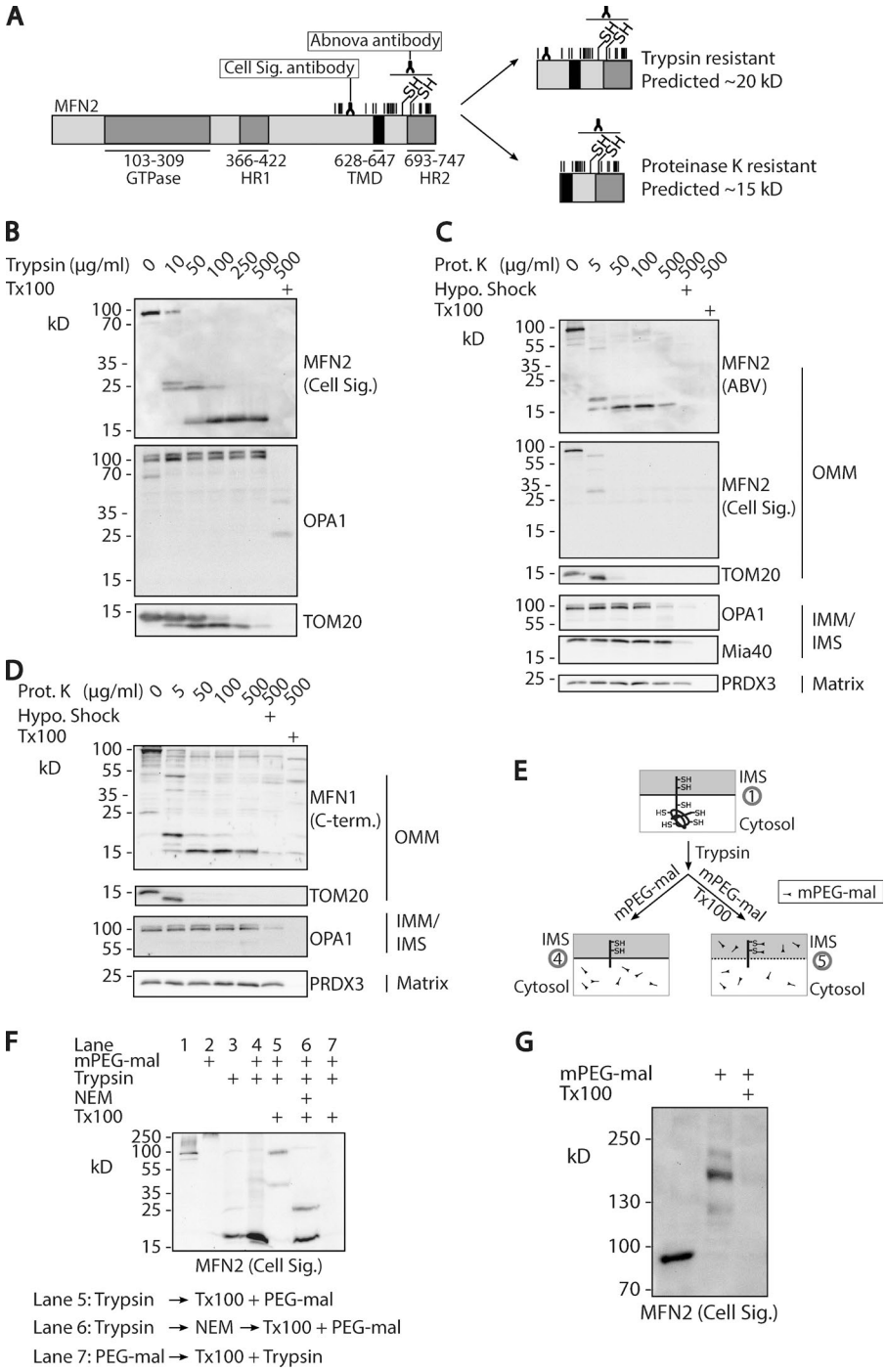

Figure 2. **Mfn C-terminal domain is protected against protease digestion and alkylation. (A)** Scheme showing predicted Mfn2 domains including the GTPase, HR1, HR2, and the predicted TMD (Liesa et al., 2009). Trypsin cut sites (predicted by PeptideCutter) are shown by vertical lines above Mfn2 scheme, specifically within the C-terminal region. The antigenic regions recognized by the two antibodies are indicated. Predicted molecular weights of protected fragments after the two protease treatments are shown, along with the antibody epitopes. Only a single predicted trypsin site resides between the Cell Signaling Technology epitope and the TMD. **(B)** Trypsin protease protection experiment. Isolated mitochondria from HEK293 cells were incubated with specified trypsin concentrations for 20 min on ice. As a control, 1% Triton X-100 was added with trypsin (last lane). Trypsin was inhibited with SBTI, and samples were processed for SDS-PAGE and immunoblotted with anti-Mfn2 (Cell Signaling Technology), anti-OPA1 (IMS), and anti-TOM20 (outer membrane). **(C and D)** Proteinase K protection experiment examining Mfn2 (C) and Mfn1 (D) topologies. Isolated mitochondria from HEK293 cells were incubated with increasing amounts of proteinase K (PK) on ice. As controls, mitochondria were treated with PK under hypotonic shock, which disrupts outer membrane while keeping inner membrane intact, or in the presence of 1% Triton X-100. PK was inhibited by PMSF, before samples were processed for Western blotting and immunoblotted with the specified antibodies. **(E)** Model illustrating the treatments used in the mPEG-maleimide experiments. After trypsin treatment, PEG-mal (indicated in the legend) can conjugate only to free cysteine residues exposed on the cytosolic face of the mitochondrial outer membrane (shown as –SH). Upon detergent solubilization, all cysteine residues become exposed. **(F)** PEGylation assay. Isolated mitochondria from HEK293 cells were treated with 10 kD mPEG-mal, which reacts with cysteine residues and shifts full-length Mfn2 into higher-molecular-weight conjugates (lane 2; also see G). Digestion with 500 μg/ml trypsin is shown in lane 3, revealing the protected fragment. Mitochondria treated with mPEG-mal followed by trypsin digestion did not show any shift in the protected fragment (lane 4). However, the trypsin-protected fragment was lost when mPEG-mal was added in the presence of Triton X-100 to solubilize the membranes (lane 5). Treating trypsin-digested mitochondria with *N*-ethylmaleimide (NEM; lane 6), which reacts with cysteines before the treatment with mPEG-mal, rescued the loss of the fragment caused by mPEG-mal treatment in lane 5. The addition of trypsin in the presence of detergent led to digestion of the fragment, confirming that the fragment is protease sensitive in solubilized lysates (lane 7). **(G)** To test whether PEGylation of the C-terminal domain results in a loss of antigenicity in the absence of trypsin, intact mitochondria were treated with mPEG-mal in the absence (lane 2) or presence (lane 3) of detergent and loaded on a 6% SDS-PAGE gel. Full-length Mfn2 shifts up upon PEGylation (lane 2). In the presence of detergent, the antibody loses immunogenicity and Mfn2 PEGylated bands disappear (lane 3).

To complement the protease protection experiments, we tested whether cysteine residues within the newly predicted IMS domain of Mfn2 were accessible to modification upon addition of 10 kD methoxypolyethyleneglycol maleimide (mPEG-mal; Fig. 2 E), a molecule that cannot pass the voltage-dependent anion-selective channel (VDAC) pores within the outer mitochondrial membrane (Colombini, 1980). Using the Cell Signaling Technology antibody against Mfn2, we observed the expected shift in molecular weight of full-length protein upon addition of mPEG-mal to isolated mitochondria (Fig. 2, F and G, lanes 1 and 2; and Fig. S2, C, D, and F). Addition of trypsin again revealed the accumulation of the ~20-kD protected fragment of Mfn2 in the absence of mPEG-mal (Fig. 2 F and Fig. S2, C and F, lane 1 vs. 3). This fragment was degraded in the presence of detergent (Fig. 2 F, lane 7; and Fig. S2, C and F). Importantly, upon addition of mPEG-mal to trypsin-treated mitochondria,

there was no change in the short fragment of Mfn2, indicating that the C-terminal cysteine residues remain inaccessible to the probe (Fig. 2 F, lane 3 vs. 4; and Fig. S2, C and F). However, addition of mPEG-mal in the presence of detergent (Triton X-100) after the quenching of trypsin activity led to the appearance of shifted bands of ∼35 and ∼100 kD that showed greatly reduced antigenicity (Fig. 2 F, lane 4 vs. 5; and Fig. S2, C and F). This 10-kD mPEG-mal conjugation of the 20-kD Mfn2 fragment was prevented by pretreatment with membrame-permeable *N*-ethyl maleimide (Fig. 2 F, lane 6). This trend was also seen with full-length Mfn2, where addition of mPEG-mal and detergent led to a near complete loss of immunogenicity of the antibody (Figs. 2 G and S2 D). We further validated these results using the purified C-terminal fragment of Mfn2. Upon incubation of the recombinant protein with PEG-mal, the immunogenicity was lost using the Abnova antibody that recognizes the entire C-terminal region (Fig. S2 E). Given that the mPEG conjugates within the C-terminal cysteines are 10 kD, it is perhaps not surprising that this would interfere with recognition by both antibodies. Collectively, the data reveal a resistance of this epitope against protease (both trypsin and proteinase K) treatment, and protection against mPEG-mal conjugation, demonstrating that the C-terminal fragment of Mfn2 resides in the IMS.

This new topology positions Mfns as members of a small class of single membrane-spanning N_{out}–C_{in} proteins with >10 residues extending within the IMS, including Tom22 and Mim1/Mim2 (Yano et al., 2000; Nakamura et al., 2004; Waizenegger et al., 2005; Papić et al., 2013). Epitope tags fused to the C termini of most tail-anchored proteins are known to block protein import and assembly into the outer membrane, yet C-tagged Mfn2 constructs have been used previously (Chen et al., 2003). An examination of the topology and membrane integration of C-tagged Mfn2 revealed complete protease accessibility to the C terminus, indicating that the tag interfered with the correct insertion into the bilayer (Fig. S3, A and B). However, this construct showed a partial rescue of mitochondrial morphology in the Mfn2 knockout (KO) MEF cells (Fig. S3 C). This suggests that the IMS localization of the C-terminal domain is not essential to drive fusion, consistent with a role as a redox sensing switch.

GSSG induces mitochondrial fusion via C-terminal cysteines in Mfn2

We previously showed that the C-terminal domain contains conserved cysteine residues at C_{684} and C_{700} (Fig. 1 C) that are critical for the GSSG-induced formation of disulfide-linked oligomers (Shutt et al., 2012) and the respiratory response to oxidative stress (Thaher et al., 2017). Using a split-luciferase–based cell-free mitochondrial fusion assay, we therefore tested the redox potential that drives mitochondrial fusion to find out whether it is consistent with the redox environment within the IMS (Schauss et al., 2010; Shutt et al., 2012; Riemer et al., 2015). A titration of glutathione (GSH):GSSG within the fusion reaction showed that increasing the levels of GSSG activates the basal mitochondrial fusion reaction ∼2.5-fold, plateauing between −206 and −197 mV, consistent with the environment within the IMS (Fig. 3 A; Calabrese et al., 2017). This shows that fusion is activated under oxidizing GSH potential. Analysis of Mfn2 within these reactions on denaturing, nonreducing gels further reveals the gradual appearance of high-molecular-weight conjugates of Mfn2 with increasing GSSG, again peaking when the levels of fusion plateau (Fig. 3 B).

Cellular stress promotes hyperfusion (Tondera et al., 2009; Shutt et al., 2012), consistent with GSSG as a molecular intermediate driving Mfn2 activation. Rather than directly adding GSSG into the reaction, we tested whether reactive oxygen species (ROS)-mediated stressors may activate fusion through the generation of GSSG from GSH within the IMS. Mitochondria within the fusion assay are actively respiring through the addition of the TCA substrate succinate, allowing ATP generation. In these conditions, the addition of complex III inhibitors blocks mitochondrial fusion (Fig. 3 C), as previously reported (Mishra et al., 2014). However, addition of an exogenous source of ATP regeneration system was able to rescue the inhibition driven by complex III inhibitors (Fig. 3 C). This demonstrates that the inhibitory effects are caused by a direct requirement for ATP in mitochondrial fusion. Interestingly, when ATP is not limiting, we observe a strictly GSH-dependent stimulation of mitochondrial fusion when complex III is blocked by myxothiazol, but not antimycin A (Fig. 3, C vs. D, 30% increase ± 8.4%, $P < 0.04$). These two drugs block complex III at different sites—antimycin A generates the majority of ROS within the matrix and myxothiazol generates ROS primarily within the IMS (Bleier and Dröse, 2013)—indicating that IMS ROS more efficiently promotes fusion. The dependence on GSH in the reaction indicates that ROS generated at complex III must be converted to GSSG to promote fusion.

We next tested whether external ROS generated within the cytosol would have a similar effect. To this end, we added an established ROS generating system (xanthine oxidase/xanthine) into the fusion reaction (Fig. 3 E; Vergun et al., 2001). With increasing concentrations of xanthine oxidase, we observed a saturable, approximately twofold stimulation of mitochondrial fusion, again dependent on the addition of GSH. We also followed the corresponding shifts of Mfn2 into disulfide-mediated oligomers for each of these conditions, resolving the complexes again on denaturing, nonreducing gels (Fig. 3 F). As previously observed, direct addition of 1 mM GSSG to the reaction led to the formation of Mfn2 oligomers and promoted fusion (Fig. 3, A [fusion] and F [far right lane]). Interestingly, increasing concentrations of xanthine oxidase led to a dose-dependent appearance of higher-order Mfn2 complexes only in the absence of GSH. Addition of GSH resulted in the reduction of these stable, disulfide-linked complexes, which coincided with the stimulation of mitochondrial fusion. This suggested a role for GSH to recycle the GSSG-induced oligomers, i.e., reducing the disulfide bonds between them, to promote multiple rounds of fusion (Riemer et al., 2015). To test this idea, we first incubated isolated mitochondria with GSSG to form stable Mfn2 disulfide-linked oligomers, and chased the reaction with GSH over 40 min (Fig. 4 A). The data show a GSH-induced loss of the disulfide-linked Mfn2 oligomers, demonstrating the gradual, reversible nature of these molecular transitions over time. Together, the data indicate that activating the Mfn2 redox cycle further activates fusion.

To understand the mechanisms and regulation of the Mitofusins, it was essential to establish the topology across the bilayer. Contrary to the accepted model with two membrane-spanning domains, Mfns instead carry a single membrane-spanning topology with conserved redox-regulated cysteine resides and the HR2 domain exposed to the IMS (Fig. 4 B). The single membrane-spanning topology can be traced to the common ancestor of animals and their closest unicellular relatives; however, the conserved cysteine residues are

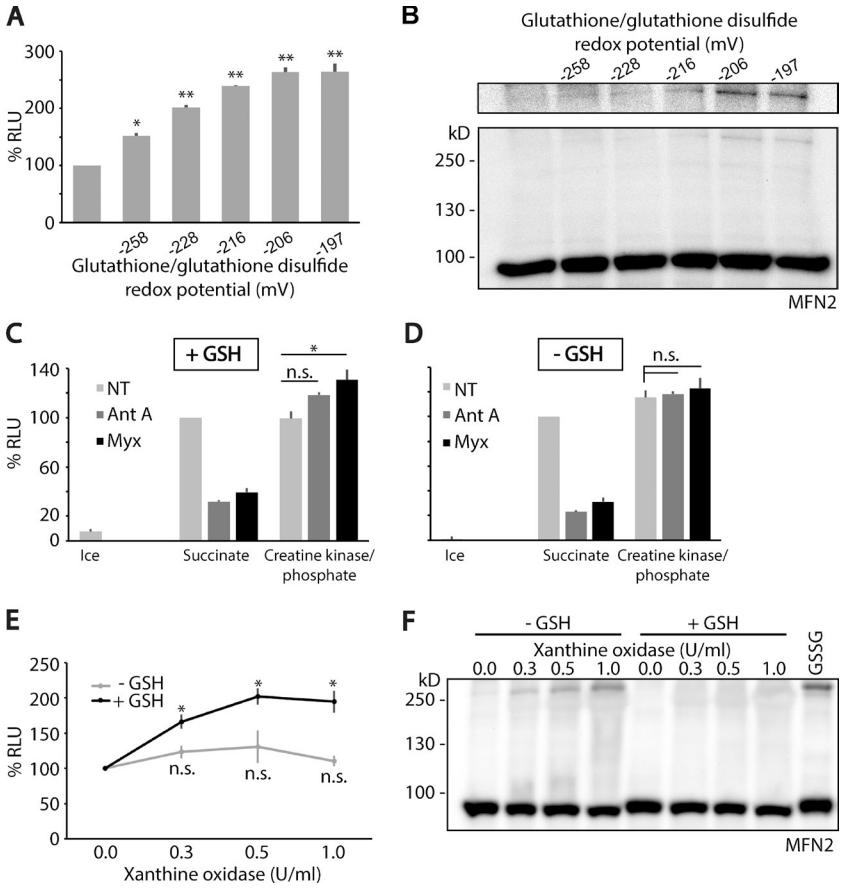

Figure 3. **Mfn2 is a sensor of mitochondria oxidative stress through GSSG, which activates mitochondrial fusion. (A)** Mitochondria containing each half of the matrix-targeted split-luciferase probes were incubated within the cell-free fusion assay system with different ratios of GSH:GSSG, corresponding to increasing GSH redox potential. Mitochondrial fusion under these conditions was quantified by measuring luciferase activity. Luciferase counts were normalized to standard condition. Fusion is activated as the potential becomes oxidizing. Reported values are the mean of three biological replicates, each performed in duplicate. Error bars are means ± SEM. **(B)** Fusion samples from A were analyzed under denaturing, nonreducing SDS-PAGE followed by immunoblotting against Mfn2 (Abnova). This gel system denatures proteins yet preserves disulfide bonds. A gradual appearance of Mfn2 disulfide oligomers was observed corresponding to fusion activation. **(C and D)** Mitochondrial fusion assays were performed with succinate to drive respiration. This reaction for 30 min at 37°C was set as the basal 100%, against which the other reactions were normalized. Reactions performed with succinate at 4°C are shown (Ice). Alternatively, an exogenous ATP regeneration system, creatine kinase and its substrate creatine phosphate, was added in place of succinate, which was sufficient for fusion (NT [gray bars], succinate vs. creatine kinase/phosphate). Mitochondria under each condition were treated with complex III inhibitors (1 µM antimycin A or 0.4 µM myxothiazol) to produce ROS in the presence (C) or absence (D) of 4 mM GSH to drive the formation of GSSG. When respiration and ATP production were driven by succinate, fusion was inhibited under these conditions. The addition of exogenous ATP regeneration system rescued the inhibition of fusion inhibition caused by blocking complex III by antimycin A (Ant A) and myxothiazol (Myx). In the presence of exogenous ATP, fusion was activated upon complex III inhibition, as long as GSH was present (C). Reported values are the mean of three biological replicates, each performed in duplicate. Error bars are means ± SEM. **(E)** Extramitochondrial ROS activates fusion in a GSH-dependent manner. Mitochondria were incubated in the presence of increasing amounts of xanthine oxidase/xanthine, which produces ROS enzymatically. In the absence of GSH, mitochondrial fusion was not activated significantly by ROS (light gray). In the presence of 4 mM GSH, fusion was activated gradually, corresponding to increasing specific activity of xanthine oxidase (black). Reported values are the mean of three biological replicates, each performed in duplicate. Error bars are means ± SEM. **(F)** Fusion samples from E were processed for denaturing, nonreducing SDS-PAGE, followed by immunoblotting with anti-Mfn2 antibody (Abnova). One additional sample was included of mitochondria incubated with 1 mM GSSG as a positive control for the formation of Mfn2 disulfide oligomers. Statistical significance was analyzed using unpaired Student's *t* test. *, $P < 0.05$; **, $P < 0.01$; n.s., not significant.

not found in these unicellular relatives or fungi, suggesting that redox-regulated mitochondrial fusion evolved as an adaptation to multicellularity in animals.

This new topology is somewhat surprising because it has been widely assumed that Mfn topology is equivalent to the yeast Fzo1 (Santel and Fuller, 2001; Rojo et al., 2002). In addition, structural information has been obtained with this assumption; namely, where HR1 and HR2 form intra- and intermolecular coiled-coil interactions (Koshiba et al., 2004; Huang et al., 2011; Franco et al., 2016; Qi et al., 2016; Cao et al., 2017). Two crystal structures were solved for an engineered fragment of Mfn1 from which ∼300 residues spanning the TMD were deleted, splicing the terminal ∼45 residues of the HR2 domain into the HR1 domain (Qi et al., 2016; Cao et al., 2017). However, data presented here demonstrate that HR1 and HR2 are instead located on either side of the outer membrane, where these direct interactions could not take place. This is in contrast to fungal Fzo1, where the presence of two clear TMDs ensures that HR2 is exposed to the cytosol, with a ∼10-aa loop within the IMS. As we showed previously (Shutt et al., 2012), and expand on here, HR2 within Mfn2 is highly redox regulated, consistent with the unique use of disulfide-switching mechanisms to regulate function within the IMS (Riemer et al., 2015). Modeling the C-terminal 110 residues reveals a highly unstructured region of ∼50 residues, linked to the coiled-coil HR2 region (Fig. 4 B). The two conserved cysteine residues lie at the junction between these two topological regions, suggesting that the generation of disulfide linkages would lead to significant conformational changes. We envision a model whereby Mfn may be operating within a dynamic cycle of oxidized and reduced disulfide complexes to promote fusion under physiological conditions. Consistent with this, the addition of GSH to preformed GSSG-induced oligomers of Mfn2 (Fig. 4 A) demonstrates that the oligomers are readily reversible in the presence of GSH. This disulfide "priming" event could allow the recycling of Mfn complexes to ensure further rounds of fusion. The action of glutaredoxin and GSH reductases on this process remain to be determined (Fischer et al., 2013; Kojer et al., 2015; Riemer et al., 2015; Kanaan et al., 2017), as does the precise composition of the disulfide-induced oligomers (Fig. 4 B). Altogether, the characterization of Mfn topology within the outer membrane provides a new conceptual understanding of the mechanisms that activate mitochondrial fusion. Future work will seek to better understand the nature of the disulfide-linked Mfn2 complex and how it is recycled to drive mitochondrial fusion.

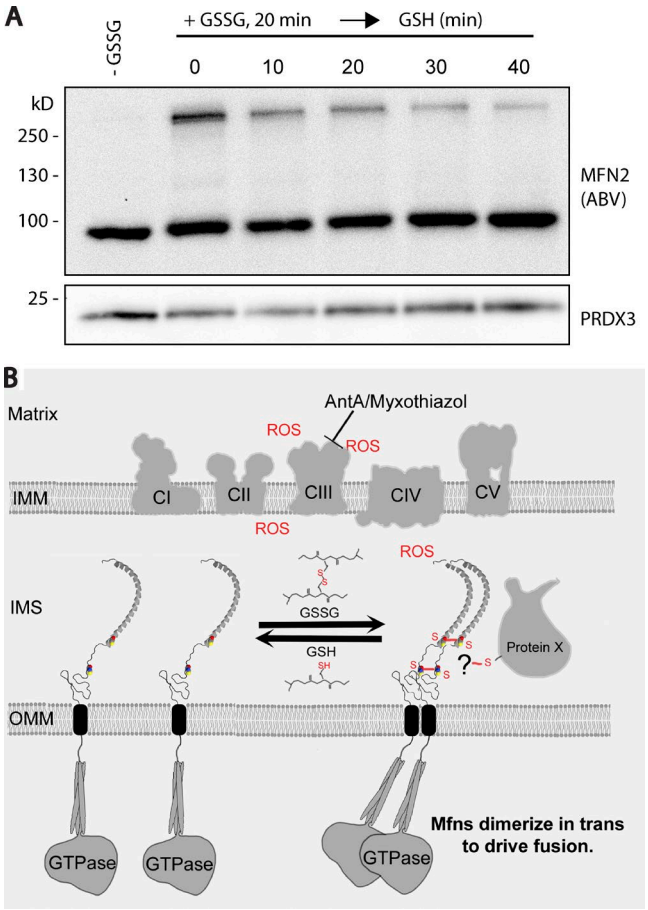

Figure 4. **Reduced GSH recycles back Mfn2 disulfide-conjugated complexes to monomeric form. (A)** Isolated mitochondria were incubated at 37°C in the absence or presence of GSSG, followed by the addition of GSH and incubation for the specified time. The samples were processed for SDS-PAGE under denaturing, nonreducing conditions and immunoblotting with Mfn2 and PRDX3 as control. **(B)** Model of mitochondrial fusion. ROS, produced from within or outside the mitochondria, activate fusion in the presence of GSH through GSSG formation. In the presence of GSSG, fusion protein Mfn2 forms disulfide-conjugated oligomers. The identity of the proteins to which Mfn2 is conjugated remains to be shown. However, Mfn2 is conjugated either to itself, forming homo-oligomers, or to another protein in the IMS. Nonetheless, the disulfide conjugation may lead to conformational changes that promote tethering or changes in GTPase activity. Notably, Mfn2 is recycled back from the GSSG-induced high-molecular-weight complexes by GSH, making the process dynamic. This recycling may prime mitochondria to go through another fusion event. The structure of the C-terminal tail of Mfn2 was predicted using Protein Structure Prediction Server [(PS)^2] v.3.0 (Huang et al., 2015), and the two C-terminal cysteines are presented in a space-fill scheme using Jmol (http://jmol.sourceforge.net/).

Materials and methods

Homology searching, phylogenetic reconstruction, and other bioinformatic methods

Characterized human Mitofusin and yeast Fzo1 sequences were used as BLAST queries to identify closely related animal and fungal sequences. Surprisingly, the top nonholozoan hits for Mfns and nonfungal hits for Fzo were BDLPs. This prompted us to entertain the hypothesis that Mfns and Fzos may have arisen independently from horizontal gene transfers of different BDLPs. To test this hypothesis, hidden Markov models (HMMs) based on Mfn and Fzo sequences obtained from diverse animal and fungal genomes were used to search for Mfn- and Fzo-related sequences using HMMer v.3.0 (Eddy, 2011) in diverse prokaryote, holozoan, and fungal genomes. Sequences retrieved with an E-value score $<1 \times 10^{-10}$ for either HMM were retained for phylogenetic analysis. Sequences were aligned by MUSCLE (Edgar, 2004) and manually adjusted and trimmed. Phylogenetic reconstructions were performed using MrBayes v.3.2 (posterior probability; Ronquist and Huelsenbeck, 2003) and RaxML v.8.2 (maximum likelihood; Stamatakis, 2006). Mfn and Fzo proteins were subjected to bioinformatic analysis using TMHMM2.0 (Krogh et al., 2001) and COILS (Lupas, 1996) to predict TMDs and coiled-coil domains, respectively. In the case of TMHMM2.0, each protein was analyzed individually. Only one animal sequence (*Caenorhabditis elegans*) was strongly predicted to have two TMDs. Because TMHMM2.0 is trained on more canonical membrane proteins than mitochondrial outer membrane proteins, it likely incorrectly predicted some of the more divergent sequences (e.g., *H. sapiens* Mfn1; see Fig. 1 B). Manual inspection of aligned sequences suggests that all fungal Fzo1 proteins have two TMDs, whereas all animal Mfn proteins have a single TMD (including the aberrantly predicted *C. elegans* Mfn protein). TMD prediction results for representative proteins are depicted (Fig. 1 B, gray lines). In the case of COILS, alignments consisting of all Fzo1 proteins and all Mfn proteins were subjected to analysis. Results from the 28-residue window with a score >0.7 were depicted against the respective sequences (Fig. 1 B, orange lines).

Materials

The following antibodies were obtained: rabbit anti-Mfn2 (#11925; Cell Signaling Technology; for both Western blot and immunofluorescence [IF]); mouse anti-Mfn2 (H00009927-M01 and H00009927-M03; Abnova); rabbit anti-Mfn1 (R. Youle, National Institutes of Health, Bethesda, MD); mouse anti-OPA1 (612607; BD Transduction Laboratories); rabbit anti-TOM20 (sc-11415; Santa Cruz Biotechnology; for both Western blot and IF); Porin (AB14734; Abcam); succinate dehydrogenase complex flavoprotein subunit A (SDHA; AB14715; Abcam); Myc (SC-40 clone 9E10; Santa Cruz Biotechnology; for both Western blot and IF); Cytc (556432; BD; for IF). Triton X-100 (X100), trypsin (T4549), soybean trypsin inhibitor (SBTI; T9003), reduced GSH (G6529), oxidized GSH (G4376), proteinase K (P8044; P2308), and creatine kinase (C3755; C7886) were obtained from Sigma-Aldrich. 10-kD mPEG-mal was obtained from JenKem Technology (M-MAL-10K). PMSF was obtained from Calbiochem (S2332). For IF, goat anti–mouse and goat anti–rabbit IgG Alexa Fluor were used as secondary antibodies (Molecular Probes). For transient transfection, cells were transfected using Lipofectamine 2000 (Invitrogen) according to the manufacturer's recommendations. Previously described cDNA encoding Mfn2-16xMyc1xHis was obtained from Addgene (plasmid 23213; deposited by D. Chan).

Cloning, expression, and purification of Mfn2 565–757 and Mfn2 648–757

Mfn2 fragments were amplified by PCR from a plasmid containing full-length Mfn2 gene. The following primers containing desired restriction sites were used: 648, BamHI, 5′-AAAGGATCCGAGCGT CTGACCTGGACCAC-3′; 565, BamHI, 5′-AAAGGATCCGCCTTG ATGGGCTACAATGAC-3′; and 648 and 565, EcoRI, 5′-AAAGAA TTCTCTGCTGGGCTGCAGGTAC-3′.

Purified PCR products and pGEX 4T1 empty vector were digested with BamHI-HF and EcoRI-HF (NEB). After gel extraction, the digested construct and vector were ligated and transformed into BL21 competent cells and plated on ampicillin lysogeny broth (LB) agar plates. Bacterial colonies were tested for insert. Bacterial preculture containing either

GST-Mfn2(565–757) or GST-Mfn2(648–757) were grown in LB (100 µg/ml ampicillin) at 37°C. When OD_{600} was ∼0.5, IPTG was added to induce expression for 2–3 h. Cells were harvested by centrifugation and broken by sonication on ice. Triton X-100 was added to 1%, and lysate was precleared by centrifugation. Supernatant was added to GSH Sepharose 4B slurry to purify GST-tagged Mfn2 fragments and incubated at RT for 10 min. After the beads were washed three times with 1% Triton X-100/PBS, batch thrombin cleavage was done overnight. The supernatant containing the cleaved product was saved and flash-frozen at −80°C.

Mitochondrial isolation

Mitochondria were isolated from suspension HeLa cells (sHeLa) stably expressing either N-MitoVZL or C-MitoLZV as described previously (Schauss et al., 2010). In brief, sHeLa were grown in 2-liter flasks in suspension MEM and harvested by centrifugation for 20 min at 4°C at 3000 *g*. Cells were broken using a Dounce homogenizer. Nuclei were centrifuged at 600 *g* for 10 min at 4°C and the postnuclear supernatant was centrifuged for 15 min at 8000 *g* at 4°C. The pellet was washed in isolation buffer (220 mM mannitol, 68 mM sucrose, 80 mM KCl, 0.5 mM EGTA, 2 mM $MgAc_2$, and 10 mM Hepes, pH 7.4), then resuspended in isolation buffer containing 10% glycerol and snap-frozen in liquid nitrogen for storage at −80°C.

Mitochondrial fusion assay

The in vitro fusion assay was performed in a 96-well plate, which was modified from Schauss et al. (2010). In brief, 20 µg of each mitochondrial population was added per reaction (25 µl) containing 15 mM Hepes, pH 7.4, 110 mM mannitol, 68 mM sucrose, 80 mM KCl, 0.5 mM EGTA, 2 mM $Mg(CH_3COO)_2$, 0.5 mM GTP, 2 mM K_2HPO_4, 1 mM ATP(K^+), and 0.08 mM ADP. The ATP regeneration system was driven by the addition of 5 mM Na succinate, or in the presence of creatine kinase/phosphate, as indicated. Reactions were assembled on ice in a 96-well plate. A previously described initial centrifugation step to concentrate mitochondria was removed (Meeusen et al., 2004; Schauss et al., 2010; Hoppins et al., 2011). After assembling the reactions, samples were incubated for 30 min at 37°C, followed by immediate solubilization and addition of substrate to quantify luciferase activity (reflecting assembly of the complementary split-luciferase polypeptides) using the *Renilla* luciferase assay kit (Promega).

Trypsin and proteinase K digestion protection experiment

Mitochondria (1 mg/ml) were isolated from HEK293 cells and incubated with specified trypsin concentrations for 20 min on ice. SBTI (5 mg/ml) was added and incubated for another 20 min on ice. Laemmli sample buffer was added, and samples were boiled for 5 min and processed for standard Western blotting analysis. For proteinase K experiments, 1 mg/ml freshly isolated mitochondria were incubated with specified concentrations of proteinase K for 30 min on ice, followed by addition of 4 mM PMSF and incubation for 20 min. For hypotonic shock control, the mitochondrial pellet was resuspended in 20 mM Hepes, pH 7.4, to cause inner membrane swelling, which was treated with proteinase K. Samples were separated on 12% SDS-PAGE gels (unless otherwise indicated in the figure legends) and processed for Western blotting as for the trypsin experiment.

Triton X-100, alkaline carbonate, and urea extractions

25 µg mitochondria isolated from nontransfected or Mfn2-16xMyc–transfected HEK293 cells were centrifuged at 8,000 *g* for 10 min. The mitochondrial pellet was resuspended in 100 µl of 1% Triton X-100 (prepared in isolation buffer), 100 µl 100 mM alkaline carbonate, pH 12, or 100 µl urea extraction buffer (4.5 M urea, 150 mM KCl, 1 mM DTT, and 20 mM Hepes, pH 7.4). Samples were incubated on ice for 30 min. Alkaline carbonate samples were vortexed briefly a few times, then centrifuged at 200,000 *g* and 4°C for 15 min. Supernatants were transferred to new microfuge tubes, and pellets were resuspended in appropriate buffers. Sample buffer was added, and samples were processed for Western blotting.

Table 1. **Concentrations of GSH and GSSG with the calculated Δ*E***

[GSH]	[GSSG]	Δ*E*
mM	*mM*	*mV*
4	0.01	−258
4	0.1	−228
4	0.25	−216
4	0.5	−206
4	1	−197

mPEG-mal experiment

We used 10-kD mPEG-mal to avoid leakage through VDAC (Colombini, 1980) and ensure that only protein regions facing the cytosol could be conjugated. Samples were kept on ice throughout the experiment. 25 µg mitochondria (1 mg/ml) isolated from HEK293 cells was incubated with 1 mM 10-kD mPEG maleimide for 1 h (or isolation buffer for controls). Excess mPEG-mal was neutralized by adding 25 mM DTT. Samples were then centrifuged for 10 min at 8,000 *g* and 4°C. Pellets were resuspended in isolation buffer and trypsin (0.5 mg/ml) where indicated, followed by inhibition of trypsin with 2 mM PMSF and 1 mM SBTI, for 20 min on ice.

For solubilization of mitochondria, Triton X-100 was added to a final concentration of 1%. Additional treatments performed on trypsinized mitochondria were done after complete inactivation of the trypsin with 1 mg/ml SBTI. Samples were boiled for 3 min after addition of sample buffer and processed for Western blotting.

GSH redox potential determination that activates fusion

GSH:GSSG ratios were used to calculate the GSH redox potential at pH 7.4 that promotes fusion using a modified Nernst equation as shown by (Dalton et al., 2004):

$$\Delta E = \left[-240\,\text{mV} + (-61.5\,\text{mV}/2e^-) \times (\text{actual pH} - 7.0)\right] - (61.5\,\text{mV}/2e^-) \times \log([\text{GSH}]2/[\text{GSSG}]).$$

GSH was added to a concentration of 4 mM, and increasing concentrations of GSSG were added to create various GSH:GSSG ratios. The concentrations of GSH and GSSG with the calculated Δ*E* are reported in Table 1.

Western blotting under denaturing, nonreducing conditions

To visualize disulfide-linked Mfn2 oligomers, sample buffer containing 50 mM iodoacetamide (with no reducing agents) was added to samples after 30-min fusion assay. Iodoacetamide will react with free cysteine residues, blocking against nonspecific reactions during sample preparation (Wrobel et al., 2016). Samples were boiled for 3 min and processed for Western blotting analysis.

Acrylamide gel purification of Mfn2(565–757)

To remove contaminating GST and GST-Mfn2(565–757) and isolate only the pure, cleaved fragment of Mfn2(565–757), we separated the recombinant preparation on a 4–16% SDS-PAGE with denaturing/

reducing conditions, and the region between molecular markers 25 and 15 was excised and chopped into small pieces. These pieces were washed three times, 5 min each at RT, with PBS and then with water. The gel was further minced with a razor and placed in an Eppendorf tube. 300 µl PBS with 0.1% SDS was added. It was sonicated on ice three times for 30 s each with rests in between. The gel was then centrifuged and the supernatant was collected. This contained the purified fragment.

Immunofluorescence microscopy and morphology quantification

MFN2-KO cells were reverse transfected with empty plasmid, untagged Mfn2, or Mfn2-16xMyc, then seeded into 24-well plates on glass coverslips. 750 ng plasmid DNA (750 ng empty plasmid, 50 ng Mfn2 supplemented with 700 ng empty plasmid, or 50 ng Mfn2-16xMyc supplemented with 700 ng empty plasmid) was diluted in 50 µl OptiMEM. 2 µl Lipofectamine 2000 was diluted in 50 µl OptiMEM, separately, for each condition. After 5-min incubation, the diluted DNA was mixed with the Lipofectamine and incubated for 15–20 min at RT. During incubation, Mfn2-KO MEFs were trypsinized, and 30,000 cells were added to each well. The DNA–Lipofectamine complexes were added to the cells in the wells. After 17 h, cells were fixed and processed for IF. For IF, cells were fixed in 5% PFA in PBS, at 37°C for 15 min, then washed three times with PBS, followed by quenching with 50 mM ammonium chloride in PBS. After three washes in PBS, cells were permeabilized in 0.1% Triton X-100 in PBS, followed by three washes in PBS. The cells were blocked with 10% FBS in PBS, followed by incubation with primary antibodies (Tom20, Mfn2 + Cytc, and Myc + Tom20 for empty plasmid, Mfn2, and Mfn2-16xMyc samples, respectively) in 5% FBS in PBS for 1 h at RT. After three washes with 5% FBS in PBS, cells were incubated with appropriate secondary antibodies (1:1,000) for 30 min at RT. After three washes in PBS, coverslips were mounted onto slides using fluorescence mounting medium (Dako). Cells were imaged using a 100× objective NA1.4 on an IX83 inverted microscope (Olympus) with appropriate lasers using a spinning disc system microscope (Yokogawa) coupled to a Neo camera (Andor).

Images were taken at random of cells expressing Mfn2 or Mfn2-16xMyc. Mitochondrial morphology of cells was categorized into three categories: tubular, intermediate, and fragmented. Cells that presented a hypertubular and branched mitochondrial network were named "tubular." Cells that showed very short mitochondria were named "fragmented." Some cells had some mitochondria that were neither long and tubular, nor very short, whereas other cells contained a combination of very short and some long mitochondria; such cells were placed in the "intermediate" category.

Statistical analysis

Errors bars displayed on graphs represent the means ± SD (or SEM when specified) of at least three independent biological replicates. Statistical significance was analyzed using unpaired Student's *t* test.

Data availability

All data supporting the findings of this study are available in the article and the supplemental information files.

Online supplemental material

Fig. S1 shows the preliminary phylogenetic reconstructions of Mfns, Fzo1, and BDLPs. Fig. S2 shows an extended analysis of Mfn2 topology and epitope mapping. Fig. S3 shows the biochemical and functional characterization of C-terminally tagged Mfn2-16xMyc. Table S1 shows protein accessions retrieved in this study.

Acknowledgments

We thank Richard Youle for providing the antibody against Mfn1, Mai Nguyen for fruitful discussions, and Adam Frost (University of California, San Francisco) for his insights and assistance with structural modeling programs.

The authors declare no competing financial interests.

This work was supported by the Canadian Institutes of Health Research Operating Grants Program to H.M. McBride, Fonds de Recherche du Québec - Santé Graduate Student Fellowship to S. Mattie, a European Molecular Biology Organization Long-Term Fellowship (ALTF 761-2014) cofunded by European Commission (EMBOCO FUND2012 and GA-2012-600394) support from Marie Curie Actions to J.G. Wideman (SFB1218 TP B02) to J. Riemer.

Author contributions: All biochemical experiments were performed by S. Mattie, and the phylogenetic and bioinformatic analysis was generated by J.G. Wideman. J. Riemer advised on all redox experiments in Fig. 3. The design of experiments and manuscript preparation were performed by S. Mattie and H.M. McBride. All authors contributed to the interpretation of results and final editing of the manuscript.

Submitted: 29 November 2016
Revised: 12 July 2017
Accepted: 14 November 2017

References

Altschul, S.F., T.L. Madden, A.A. Schäffer, J. Zhang, Z. Zhang, W. Miller, and D.J. Lipman. 1997. Gapped BLAST and PSI-BLAST: A new generation of protein database search programs. *Nucleic Acids Res.* 25:3389–3402. https://doi.org/10.1093/nar/25.17.3389

Bleier, L., and S. Dröse. 2013. Superoxide generation by complex III: From mechanistic rationales to functional consequences. *Biochim. Biophys. Acta.* 1827:1320–1331. https://doi.org/10.1016/j.bbabio.2012.12.002

Calabrese, G., B. Morgan, and J. Riemer. 2017. Mitochondrial glutathione: Regulation and functions. *Antioxid. Redox Signal.* 27:1162–1177. https://doi.org/10.1089/ars.2017.7121

Cao, Y.L., S. Meng, Y. Chen, J.X. Feng, D.D. Gu, B. Yu, Y.J. Li, J.Y. Yang, S. Liao, D.C. Chan, and S. Gao. 2017. MFN1 structures reveal nucleotide-triggered dimerization critical for mitochondrial fusion. *Nature.* 542:372–376. https://doi.org/10.1038/nature21077

Chen, H., S.A. Detmer, A.J. Ewald, E.E. Griffin, S.E. Fraser, and D.C. Chan. 2003. Mitofusins Mfn1 and Mfn2 coordinately regulate mitochondrial fusion and are essential for embryonic development. *J. Cell Biol.* 160:189–200. https://doi.org/10.1083/jcb.200211046

Colombini, M. 1980. Structure and mode of action of a voltage dependent anion-selective channel (VDAC) located in the outer mitochondrial membrane. *Ann. N. Y. Acad. Sci.* 341(1 Anion and Pro):552–563. https://doi.org/10.1111/j.1749-6632.1980.tb47198.x

Dalton, T.P., Y. Chen, S.N. Schneider, D.W. Nebert, and H.G. Shertzer. 2004. Genetically altered mice to evaluate glutathione homeostasis in health and disease. *Free Radic. Biol. Med.* 37:1511–1526. https://doi.org/10.1016/j.freeradbiomed.2004.06.040

Davies, V.J., A.J. Hollins, M.J. Piechota, W. Yip, J.R. Davies, K.E. White, P.P. Nicols, M.E. Boulton, and M. Votruba. 2007. Opa1 deficiency in a mouse model of autosomal dominant optic atrophy impairs mitochondrial morphology, optic nerve structure and visual function. *Hum. Mol. Genet.* 16:1307–1318. https://doi.org/10.1093/hmg/ddm079

Eddy, S.R. 2011. Accelerated profile HMM searches. *PLOS Comput. Biol.* 7:e1002195. https://doi.org/10.1371/journal.pcbi.1002195

Edgar, R.C. 2004. MUSCLE: A multiple sequence alignment method with reduced time and space complexity. *BMC Bioinformatics.* 5:113. https://doi.org/10.1186/1471-2105-5-113

Fischer, M., S. Horn, A. Belkacemi, K. Kojer, C. Petrungaro, M. Habich, M. Ali, V. Küttner, M. Bien, F. Kauff, et al. 2013. Protein import and oxidative folding in the mitochondrial intermembrane space of intact mammalian cells. *Mol. Biol. Cell.* 24:2160–2170. https://doi.org/10.1091/mbc.E12-12-0862

Franco, A., R.N. Kitsis, J.A. Fleischer, E. Gavathiotis, O.S. Kornfeld, G. Gong, N. Biris, A. Benz, N. Qvit, S.K. Donnelly, et al. 2016. Correcting mitochondrial fusion by manipulating mitofusin conformations. *Nature.* 540:74–79. https://doi.org/10.1038/nature20156

Hoppins, S., F. Edlich, M.M. Cleland, S. Banerjee, J.M. McCaffery, R.J. Youle, and J. Nunnari. 2011. The soluble form of Bax regulates mitochondrial fusion via MFN2 homotypic complexes. *Mol. Cell.* 41:150–160. https://doi.org/10.1016/j.molcel.2010.11.030

Huang, P., C.A. Galloway, and Y. Yoon. 2011. Control of mitochondrial morphology through differential interactions of mitochondrial fusion and fission proteins. *PLoS One.* 6:e20655. https://doi.org/10.1371/journal.pone.0020655

Huang, T.T., J.K. Hwang, C.H. Chen, C.S. Chu, C.W. Lee, and C.C. Chen. 2015. (PS)2: Protein structure prediction server version 3.0. *Nucleic Acids Res.* 43(W1):W338–W342. https://doi.org/10.1093/nar/gkv454

Kanaan, G.N., B. Ichim, L. Gharibeh, W. Maharsy, D.A. Patten, J.Y. Xuan, A. Reunov, P. Marshall, J. Veinot, K. Menzies, et al. 2017. Glutaredoxin-2 controls cardiac mitochondrial dynamics and energetics in mice, and protects against human cardiac pathologies. *Redox Biol.* 14:509–521. https://doi.org/10.1016/j.redox.2017.10.019

Kojer, K., V. Peleh, G. Calabrese, J.M. Herrmann, and J. Riemer. 2015. Kinetic control by limiting glutaredoxin amounts enables thiol oxidation in the reducing mitochondrial intermembrane space. *Mol. Biol. Cell.* 26:195–204. https://doi.org/10.1091/mbc.E14-10-1422

Koshiba, T., S.A. Detmer, J.T. Kaiser, H. Chen, J.M. McCaffery, and D.C. Chan. 2004. Structural basis of mitochondrial tethering by mitofusin complexes. *Science.* 305:858–862. https://doi.org/10.1126/science.1099793

Krogh, A., B. Larsson, G. von Heijne, and E.L. Sonnhammer. 2001. Predicting transmembrane protein topology with a hidden Markov model: Application to complete genomes. *J. Mol. Biol.* 305:567–580. https://doi.org/10.1006/jmbi.2000.4315

Labbé, K., A. Murley, and J. Nunnari. 2014. Determinants and functions of mitochondrial behavior. *Annu. Rev. Cell Dev. Biol.* 30:357–391. https://doi.org/10.1146/annurev-cellbio-101011-155756

Liesa, M., M. Palacín, and A. Zorzano. 2009. Mitochondrial dynamics in mammalian health and disease. *Physiol. Rev.* 89:799–845. https://doi.org/10.1152/physrev.00030.2008

Lupas, A. 1996. Prediction and analysis of coiled-coil structures. *Methods Enzymol.* 266:513–525. https://doi.org/10.1016/S0076-6879(96)66032-7

Meeusen, S., J.M. McCaffery, and J. Nunnari. 2004. Mitochondrial fusion intermediates revealed in vitro. *Science.* 305:1747–1752. https://doi.org/10.1126/science.1100612

Meeusen, S., R. DeVay, J. Block, A. Cassidy-Stone, S. Wayson, J.M. McCaffery, and J. Nunnari. 2006. Mitochondrial inner-membrane fusion and crista maintenance requires the dynamin-related GTPase Mgm1. *Cell.* 127:383–395. https://doi.org/10.1016/j.cell.2006.09.021

Mishra, P., V. Carelli, G. Manfredi, and D.C. Chan. 2014. Proteolytic cleavage of Opa1 stimulates mitochondrial inner membrane fusion and couples fusion to oxidative phosphorylation. *Cell Metab.* 19:630–641. https://doi.org/10.1016/j.cmet.2014.03.011

Muñoz-Gómez, S.A., C.H. Slamovits, J.B. Dacks, K.A. Baier, K.D. Spencer, and J.G. Wideman. 2015. Ancient homology of the mitochondrial contact site and cristae organizing system points to an endosymbiotic origin of mitochondrial cristae. *Curr. Biol.* 25:1489–1495. https://doi.org/10.1016/j.cub.2015.04.006

Nakamura, Y., H. Suzuki, M. Sakaguchi, and K. Mihara. 2004. Targeting and assembly of rat mitochondrial translocase of outer membrane 22 (TOM22) into the TOM complex. *J. Biol. Chem.* 279:21223–21232. https://doi.org/10.1074/jbc.M314156200

Papić, D., Y. Elbaz-Alon, S.N. Koerdt, K. Leopold, D. Worm, M. Jung, M. Schuldiner, and D. Rapaport. 2013. The role of Djp1 in import of the mitochondrial protein Mim1 demonstrates specificity between a cochaperone and its substrate protein. *Mol. Cell. Biol.* 33:4083–4094. https://doi.org/10.1128/MCB.00227-13

Pareyson, D., P. Saveri, A. Sagnelli, and G. Piscosquito. 2015. Mitochondrial dynamics and inherited peripheral nerve diseases. *Neurosci. Lett.* 596:66–77. https://doi.org/10.1016/j.neulet.2015.04.001

Purkanti, R., and M. Thattai. 2015. Ancient dynamin segments capture early stages of host-mitochondrial integration. *Proc. Natl. Acad. Sci. USA.* 112:2800–2805. https://doi.org/10.1073/pnas.1407163112

Qi, Y., L. Yan, C. Yu, X. Guo, X. Zhou, X. Hu, X. Huang, Z. Rao, Z. Lou, and J. Hu. 2016. Structures of human mitofusin 1 provide insight into mitochondrial tethering. *J. Cell Biol.* 215:621–629. https://doi.org/10.1083/jcb.201609019

Riemer, J., M. Schwarzländer, M. Conrad, and J.M. Herrmann. 2015. Thiol switches in mitochondria: Operation and physiological relevance. *Biol. Chem.* 396:465–482. https://doi.org/10.1515/hsz-2014-0293

Rojo, M., F. Legros, D. Chateau, and A. Lombès. 2002. Membrane topology and mitochondrial targeting of mitofusins, ubiquitous mammalian homologs of the transmembrane GTPase Fzo. *J. Cell Sci.* 115:1663–1674.

Ronquist, F., and J.P. Huelsenbeck. 2003. MrBayes 3: Bayesian phylogenetic inference under mixed models. *Bioinformatics.* 19:1572–1574. https://doi.org/10.1093/bioinformatics/btg180

Ryan, M.T., and D. Stojanovski. 2012. Mitofusins 'bridge' the gap between oxidative stress and mitochondrial hyperfusion. *EMBO Rep.* 13:870–871. https://doi.org/10.1038/embor.2012.132

Santel, A., and M.T. Fuller. 2001. Control of mitochondrial morphology by a human mitofusin. *J. Cell Sci.* 114:867–874.

Santel, A., S. Frank, B. Gaume, M. Herrler, R.J. Youle, and M.T. Fuller. 2003. Mitofusin-1 protein is a generally expressed mediator of mitochondrial fusion in mammalian cells. *J. Cell Sci.* 116:2763–2774. https://doi.org/10.1242/jcs.00479

Schauss, A.C., H. Huang, S.Y. Choi, L. Xu, S. Soubeyrand, P. Bilodeau, R. Zunino, P. Rippstein, M.A. Frohman, and H.M. McBride. 2010. A novel cell-free mitochondrial fusion assay amenable for high-throughput screenings of fusion modulators. *BMC Biol.* 8:100. https://doi.org/10.1186/1741-7007-8-100

Shutt, T.E., and H.M. McBride. 2013. Staying cool in difficult times: Mitochondrial dynamics, quality control and the stress response. *Biochim. Biophys. Acta.* 1833:417–424.

Shutt, T., M. Geoffrion, R. Milne, and H.M. McBride. 2012. The intracellular redox state is a core determinant of mitochondrial fusion. *EMBO Rep.* 13:909–915. https://doi.org/10.1038/embor.2012.128

Stamatakis, A. 2006. RAxML-VI-HPC: Maximum likelihood-based phylogenetic analyses with thousands of taxa and mixed models. *Bioinformatics.* 22:2688–2690. https://doi.org/10.1093/bioinformatics/btl446

Thaher, O., C. Wolf, P.N. Dey, A. Pouya, V. Wüllner, S. Tenzer, and A. Methner. 2017. The thiol switch C684 in Mitofusin-2 mediates redox-induced alterations of mitochondrial shape and respiration. *Neurochem. Int.* doi:10.1016/j.neuint.2017.05.009.

Tondera, D., S. Grandemange, A. Jourdain, M. Karbowski, Y. Mattenberger, S. Herzig, S. Da Cruz, P. Clerc, I. Raschke, C. Merkwirth, et al. 2009. SLP-2 is required for stress-induced mitochondrial hyperfusion. *EMBO J.* 28:1589–1600. https://doi.org/10.1038/emboj.2009.89

Vergun, O., A.I. Sobolevsky, M.V. Yelshansky, J. Keelan, B.I. Khodorov, and M.R. Duchen. 2001. Exploration of the role of reactive oxygen species in glutamate neurotoxicity in rat hippocampal neurones in culture. *J. Physiol.* 531:147–163. https://doi.org/10.1111/j.1469-7793.2001.0147j.x

Waizenegger, T., S. Schmitt, J. Zivkovic, W. Neupert, and D. Rapaport. 2005. Mim1, a protein required for the assembly of the TOM complex of mitochondria. *EMBO Rep.* 6:57–62. https://doi.org/10.1038/sj.embor.7400318

Wrobel, L., A.M. Sokol, M. Chojnacka, and A. Chacinska. 2016. The presence of disulfide bonds reveals an evolutionarily conserved mechanism involved in mitochondrial protein translocase assembly. *Sci. Rep.* 6:27484. https://doi.org/10.1038/srep27484

Yano, M., N. Hoogenraad, K. Terada, and M. Mori. 2000. Identification and functional analysis of human Tom22 for protein import into mitochondria. *Mol. Cell. Biol.* 20:7205–7213. https://doi.org/10.1128/MCB.20.19.7205-7213.2000